ORIGINAL RESEARCH

MR Imaging of Congenital or Developmental Neuropathic Strabismus: Common and Uncommon Findings

E. Kim
J.H. Kim
J.M. Hwang
B.S. Choi
C. Jung

BACKGROUND AND PURPOSE: High-resolution MR imaging enables direct imaging of the ocular motor nerves. The aim of this study was to assess the various causes of congenital or developmental neuropathic strabismus by using high-resolution MR imaging.

MATERIALS AND METHODS: High-resolution MR imaging was performed to evaluate the ocular motor nerves (CNIII, CNIV, CNVI) in 247 consecutive patients with suspected congenital or developmental neuropathic strabismus. These MR images, along with those obtained from conventional MR imaging of the brain and the orbit, were evaluated.

RESULTS: MR imaging abnormalities were found in 112 patients: ocular motor nerve abnormalities in 98 patients (88%), orbital abnormalities in 9 patients (8%), and brain abnormalities in 5 patients (4%). Ocular motor nerve abnormalities were CNIV aplasia (63%), CNVI aplasia or hypoplasia (21%), CNIII aplasia or hypoplasia (3%), and combined CNIII aplasia and CNVI hypoplasia (1%). Orbital abnormalities were EOM hypoplasia (7%), EOM hypertrophy (1%), and fibrotic mass (1%). Brain abnormalities were periventricular leukomalacia (4%) and periventricular heterotopia (1%).

CONCLUSIONS: Various MR imaging abnormalities were associated with congenital and developmental neuropathic strabismus. The most common abnormality was CNIV aplasia.

ABBREVIATIONS: CN = cranial nerve; EOM = extraocular muscle; SENSE = sensitivity encoding; 3D-bTFE = 3D balanced turbo-field echo

Dysfunction of the ocular motor nerves (CNIII, CNIV, and CNVI), due to acquired conditions (such as trauma, tumor, inflammation, infection, and vascular lesions) and congenital or developmental diseases, can cause neuropathic strabismus. MR imaging studies of congenital or developmental neuropathic strabismus have been sporadically conducted, but most of these studies focused on the abnormalities of individual ocular motor nerves and EOMs.[1-10] To our knowledge, only Demer et al[11] and Jiao et al[12] conducted MR imaging studies to investigate the various etiologies of congenital or developmental neuropathic strabismus, including abnormalities of ocular motor nerves and EOMs. A population-based study[13] reported that CNIV palsy occurred with the highest frequency in patients with pediatric neuropathic strabismus. The study by Demer et al[11] could not consistently determine the status of CNIV, due to the relatively large voxel size of their imaging equipment, which was not appropriate for the small-sized CNIV. In addition, Jiao et al[12] did not include patients with a CNIV abnormality. CNIV is the most difficult to visualize when using MR imaging because of its small size; it has an average diameter of 0.4 mm.[14]

Recent technical improvements in MR imaging have led to the development of higher-resolution imaging, with a voxel size less than the diameter of CNIV. In recent high-resolution MR imaging studies, CNIV was consistently identified in healthy subjects but was absent in patients with congenital superior oblique palsy.[2,3,15] In our hospital, we have used an MR imaging protocol modified for examination of congenital or developmental neuropathic strabismus to evaluate CNIV as well as CNIII, CNVI, and EOMs. In this study, we analyzed common and uncommon MR imaging abnormalities in a large series of patients with congenital or developmental neuropathic strabismus.

Received December 26, 2011; accepted after revision March 2, 2012.

From the Departments of Radiology (E.K., J.H.K., B.S.C., C.J.) and Ophthalmology (J.M.H.), Seoul National University College of Medicine, Seoul National University Bundang Hospital, Seongnam-si, Korea.

Please address correspondence to Jae Hyoung Kim, MD, Department of Radiology, Seoul National University Bundang Hospital, 166 Gumi-ro, Bundang-gu, Seongnam-si, Gyeonggi-do, 463-707, Korea; e-mail: jaehkim@snu.ac.kr

http://dx.doi.org/10.3174/ajnr.A3136

Materials and Methods

Subjects

During a recent 30-month period, 1640 patients with ocular motility disorder initially visited the neuro-ophthalmology clinic of our hospital. Of the 1640 patients, 260 patients suspected of having either ocular motor neuropathy or orbital myopathy, on the basis of the clinical findings, underwent MR imaging. Thirteen patients with acquired ocular motility disorder were excluded because of ischemic or diabetic neuropathy ($n = 7$), traumatic neuropathy ($n = 2$), postinfection neuropathy ($n = 1$), clival meningioma ($n = 1$), oculomotor neuritis ($n = 1$), or neurovascular compression syndrome ($n = 1$). Therefore, a total of 247 consecutive patients with presumed congenital or developmental neuropathic strabismus were included in this retrospective study. These patients had a history of congenital or developmental strabismus without any evidence of acquired disease or head or orbital trauma. The patient population included 144 males and 103 females between the ages of 5 months and 64 years (mean, 9.5 years; median, 5 years). The distribution of patient ages was as follows: 0–3 years ($n = 59$); 3–5 years ($n = 66$); 5–10 years ($n = 67$); 10–20 years ($n = 25$); and >20 years ($n = 30$).

In our neuro-ophthalmologic clinic, visual acuity and extraocular movement tests, including the Bielschowsky head-tilt test, the ocular alignment with prism cover test in 6 cardinal positions of gaze at

distance, the maximum amount of vertical deviation at 6 cardinal gazes, laterality of the paretic eye, fixation dominance, and dissociated vertical deviation were performed in cooperative patients.

Five males and 5 females, with an age range of 6 months to 25 years (mean, 9.2 years; median, 5 years), were included as control subjects to measure the size of CNIII, CNIV, and CNVI; these controls were selected from among patients who underwent brain MR imaging for headaches without any ocular movement abnormality and who did not show any abnormality on the MR images. Informed consent for MR imaging was obtained from all subjects or their guardians, and the hospital institutional review board approved this retrospective study.

MR Imaging

MR imaging was conducted using a 3T system (Intera Achieva; Philips Medical Systems, Best, the Netherlands) with an 8-channel or a 32-channel SENSE head coil. Children younger than 6 years of age were sedated using chloral hydrate, administrated orally at 500 mg/kg. The optimized protocol for evaluation of strabismus consisted of axial T2-weighted imaging of the brain, coronal T2-weighted imaging of the orbit, conventional resolution 3D-bTFE imaging for CNIII and CNVI, and high-resolution 3D-bTFE imaging for CNIV.

Axial T2-weighted images of the brain were obtained with a turbo spin-echo sequence with the following parameters: TR/TE 3000/80 ms; echo-train length, 15; field of view, 168 × 210 mm; acquisition matrix, 364 × 280; and section thickness, 5 mm. Coronal T2-weighted imaging for the orbit was performed from the anterior-most part of the eyeball to the sellar region using a turbo spin-echo sequence with the following parameters: TR/TE, 4800/80 ms; echo-train length, 16; field of view, 150 × 150 mm; matrix, 256 × 256; and section thickness, 2 mm.

Conventional-resolution 3D-bTFE imaging for CNIII and CNVI was performed in a transverse plane from the midbrain to the upper medulla oblongata with the following parameters: TR/TE, 6.2/3.1 ms; flip angle, 60°; field of view, 150 × 150 mm; matrix, 224 × 333; section thickness, 14 mm (0.7-mm overlap with adjacent sections); voxel size, 0.67 × 0.45 × 1.4 mm; number of sections, 70; SENSE factor, 1.5; number of excitations, 2; and acquisition time, 3 minutes 39 seconds. In 5 patients, because a susceptibility artifact caused by hyperpneumatization of the sphenoid sinus was too severe to evaluate the cranial nerves, additional imaging with T2 volume isotropic turbo spin-echo acquisition (VISTA) was conducted using the following parameters: TR/TE, 2000/240 ms; flip angle, 90°; echo-train length, 70; field of view, 150 × 150 mm; matrix, 216 × 214; section thickness, 14 mm (0.7-mm overlap with adjacent sections); voxel size, 0.7 × 0.7 × 1.4 mm; number of sections, 70; SENSE factor, 2; number of excitations, 2; and acquisition time, 4 minutes 17 seconds.

High-resolution 3D-bTFE imaging for CNIV was performed at the lower midbrain and the upper pons, including the inferior margin of the inferior colliculus, which is known to be the level at which the CNIV root exits. The scanning plane was set to an oblique axial direction, perpendicular to the long axis of the aqueduct, which was approximately parallel to the course of CNIV. During the initial 25-month period, high-resolution 3D-bTFE was conducted with an 8-channel head coil and the following parameters: TR/TE, 9.9/5.0 ms; flip angle, 60°; field of view, 150 × 150 mm; acquisition matrix, 500 × 500; section thickness, 0.25 mm; voxel size, 0.3 × 0.3 × 0.25 mm; number of sections, 60; SENSE factor, 2; number of excitations, 2; and acquisition time, 7 minutes 14 seconds. For the subsequent 5 months, high-resolution 3D-bTFE was conducted using a 32-channel head coil that provided a better signal-to-noise ratio. Therefore, we reduced the acquisition time by adjusting several parameters as follows: field of view, 80 × 80 mm; matrix, 268 × 266; SENSE factor, 1.6; number of excitations, 3; and acquisition time, 4 minutes 47 seconds. The other parameters were not changed. In the patient group, 191 subjects underwent high-resolution 3D-bTFE imaging for CNIV using the initial sequence, and the remaining 56 using the latter sequence. In 8 of the control group subjects, high-resolution 3D-bTFE imaging for CNIV was performed with the initial sequence, and in the other 2 with the latter sequence.

MR imaging abnormalities in congenital or developmental neuropathic strabismus

MR Imaging Findings	Number of Patients (n = 112)
Ocular motor nerve abnormalities	98 (88%)
CNIV aplasia	71 (63%)
CNVI aplasia or hypoplasia	23 (21%)
CNIII aplasia or hypoplasia	3 (3%)
Combined CNIII hypoplasia and CNVI aplasia	1 (1%)
Orbital abnormalities	9 (8%)
Superior oblique hypoplasia	4 (4%)
Medial rectus hypoplasia	1 (1%)
Inferior rectus hypoplasia	1 (1%)
Lateral rectus hypoplasia	1 (1%)
Superior rectus hypertrophy	1 (1%)
Fibrotic mass	1 (1%)
Brain abnormalities	5 (4%)
Periventricular leukomalacia	4 (4%)
Periventricular heterotopia	1 (1%)

Image Analysis

Two radiologists specialized in head and neck imaging, with 7 and 20 years of experience, respectively, analyzed the MR images and reached a consensus. We assessed the status of the brain, EOMs, and ocular motor nerves in the same session. Axial T2-weighted images of the brain and coronal T2-weighted images of the orbit were reviewed to assess the abnormality of the brain and the orbit, respectively. The size and shape of the EOMs were visually evaluated.

From the 3D-bTFE images, aplasia of CNIII, CNIV, and CNVI in the cisternal segment was determined visually. Hypoplasia was determined by measuring the diameter of the nerves on magnified images of more than 2 times the original images using a PACS. A CNIII smaller than the acoustic nerve in diameter was determined as hypoplasia, according to the criteria suggested in a previous study.[4] To determine CNVI hypoplasia, CNIV was used as an internal reference. In 10 controls, the greatest diameters of the right and left CNVI and CNIV were measured at their cisternal segments and then averaged. The mean diameter of CNVI was 7.6 mm (range, 7.1–8.3 mm) and that of CNIV was 4.3 mm (range, 3.6–5.0 mm). Therefore, a CNVI smaller than CNIV was considered as evidence of hypoplasia. For CNIV, only the presence or absence of aplasia was assessed, because CNIV hypoplasia was difficult to determine due to its small diameter and the lack of a comparable reference.

Results

Of the 247 patients, 135 did not demonstrate any abnormality on MR imaging of the ocular motor nerves, the orbit, or the brain, whereas 112 patients showed abnormalities. Most (88%) demonstrated ocular motor nerve abnormalities, while some orbital (8%) and brain abnormalities (4%) were also observed (Table).

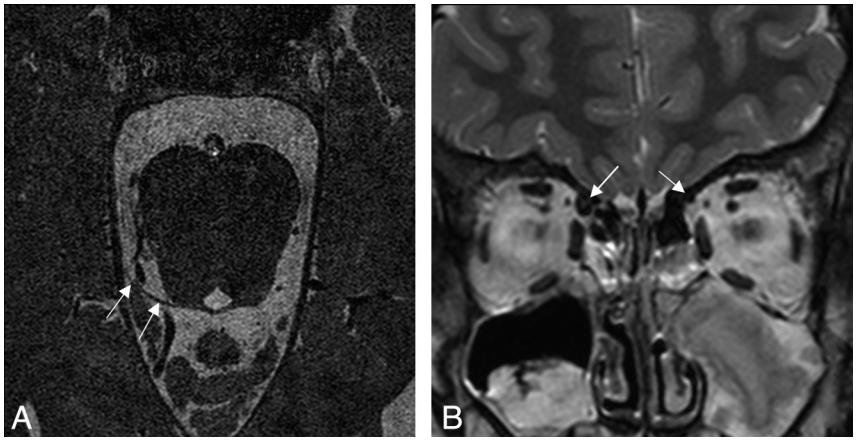

Fig 1. CNIV aplasia in a 9-year-old girl. *A*, High-resolution 3D-bTFE image with 32-channel SENSE head coil at the level of the superior medullary velum shows a normal right CNIV (*arrows*), but the left CNIV is absent. *B*, Coronal T2-weighted image of the orbit shows a hypoplastic left superior oblique hypoplasia (*small arrow*) compared with the right side (*large arrow*).

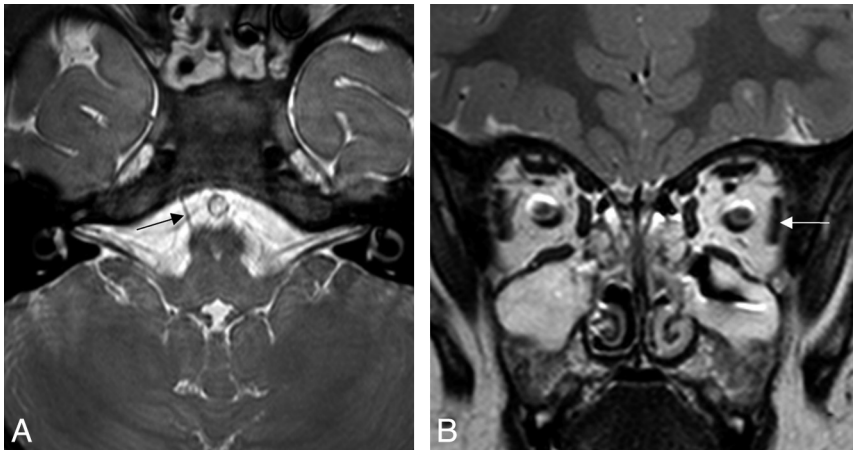

Fig 2. CNVI aplasia in a 3-year-old boy. *A*, Conventional resolution 3D-bTFE image at the level of the pontomedullary junction shows a normal right CNVI (*arrow*), but the left CNVI is absent. *B*, In a coronal T2-weighted image of the orbit, hypoplastic change is not observed in the left lateral rectus (*arrow*).

As described in the table, the patients with ocular motor nerve abnormalities were most frequently observed to have abnormalities associated with either CNIV (63%) or CNVI (21%), and relatively fewer patients showed CNIII abnormalities (3%) or abnormalities associated with both CNIII and CNVI (1%). All of the CNIV abnormalities appeared as unilateral aplasia with ipsilateral hypoplasia of the superior oblique (Fig 1). The CNVI abnormalities most frequently presented as unilateral CNVI aplasia ($n = 20$), with only a few patients showing bilateral CNVI aplasia ($n = 2$) or unilateral CNVI hypoplasia ($n = 1$) (Fig 2). CNVI aplasia or hypoplasia was not associated with hypoplasia of the lateral rectus. The CNIII abnormalities presented as unilateral CNIII aplasia with hypoplasia of all ipsilateral EOMs innervated by CNIII ($n = 1$), unilateral CNIII hypoplasia with ipsilateral hypoplasia of both the medial and inferior recti ($n = 1$), or unilateral CNIII hypoplasia with an ipsilateral hypoplastic medial rectus ($n = 1$) (Fig 3). One patient who showed combined CNIII and CNVI abnormalities had bilateral CNIII hypoplasia and bilateral CNVI aplasia associated with hypoplasia of both the bilateral superior and bilateral medial recti (Fig 4).

The orbital abnormality that was most frequently observed was unilateral superior oblique hypoplasia, which was observed in 4 patients; the other abnormalities of the orbit were unilateral medial rectus hypoplasia, bilateral inferior rectus hypoplasia, unilateral lateral rectus hypoplasia, unilateral superior rectus hypertrophy, and a fibrotic mass. In 4 patients with superior oblique hypoplasia, CNIII and CNVI were normally identified, but CNIV could not be precisely evaluated because of motion artifacts ($n = 2$) or a narrow cisternal space with poor differentiation between the nerve and vessels ($n = 2$). Although CNIV aplasia could have caused superior oblique hypoplasia observed in these patients, this hypoplasia was categorized as an orbital abnormality. Five patients with EOM abnormalities or the presence of a fibrotic mass showed normal CNIII, CNIV, and CNVI in the cisternal segment. Superior rectus hypertrophy was found in a 3-year-old boy with no clinical evidence of thyroid ophthalmopathy. The hypertrophic superior rectus was recessed and a biopsy revealed fibrotic tissue with nonspecific changes (Fig 5). The orbital fibrotic mass was adhered to the medial rectus in a 9-month-old boy, and a biopsy revealed only fibrosis.

Brain abnormalities were observed in 5 patients: periventricular leukomalacia in 4 and periventricular heterotopia in 1, all involving the periventricular white matter bilaterally including the occipital region. Of the 4 patients with periventricular leukomalacia, 3 were born prematurely and 1 was born at full term.

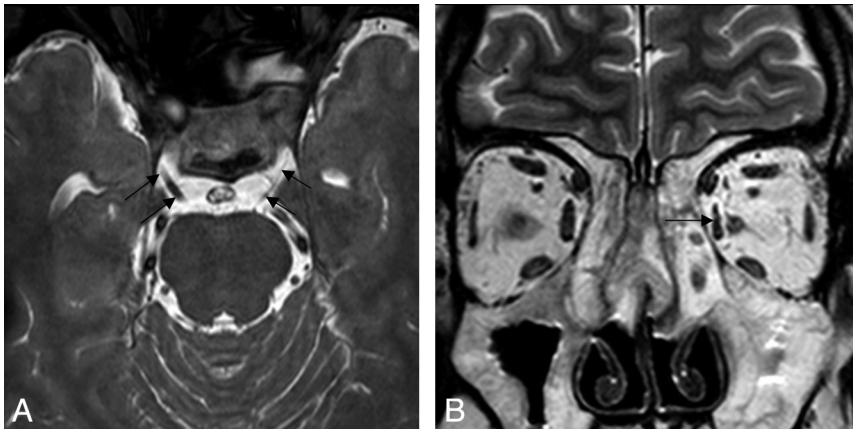

Fig 3. CNIII hypoplasia in a 38-year-old man. *A*, Conventional-resolution 3D-bTFE image at the level of the upper pons shows a hypoplastic left CNIII (*arrows*). *B*, Coronal T2-weighted image of the orbit shows a hypoplastic left medial rectus (*arrow*).

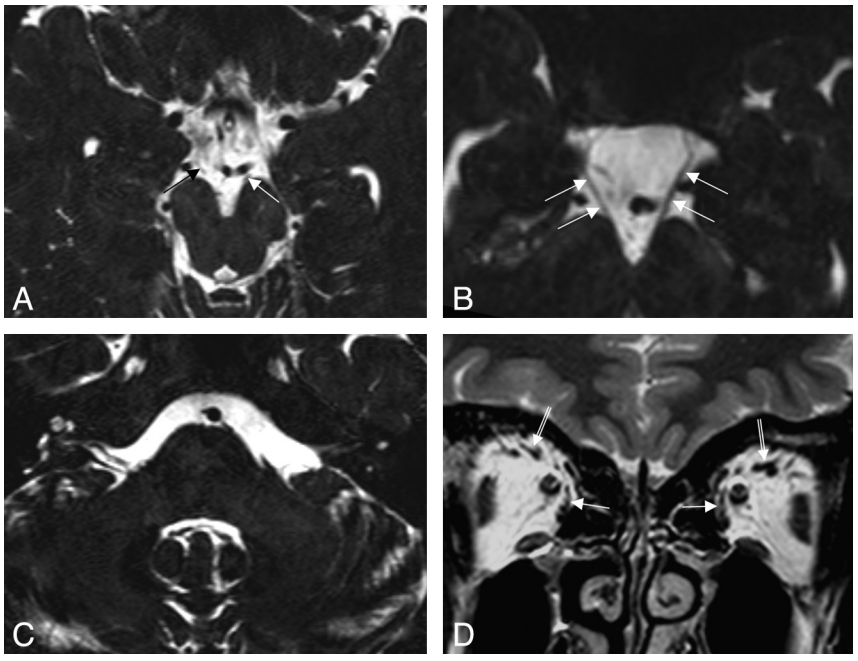

Fig 4. Bilateral CNIII hypoplasia and bilateral CNVI aplasia in a 25-year-old man. *A* and *B*, Conventional-resolution T2 VISTA images with reformation in an oblique direction (*B*) at the level of the lower midbrain, showing a hypoplastic CNIII, bilaterally (*arrows*). *C*, Conventional-resolution T2 VISTA image at the level of the lower pons shows the absence of bilateral CNVI. *D*, Coronal T2-weighted image of the orbit shows hypoplasia of the superior rectus (*double arrow*) and the medial rectus (*arrow*), bilaterally.

Discussion

Recently, steady-state coherent fast gradient-echo sequences and fast spin-echo sequences have been commonly used for cranial nerve imaging, because cranial nerves are well contrasted to the background signal intensity of the CSF and are therefore more easily identified.[16,17] The 3D-bTFE technique is based on acquiring a fast gradient-echo sequence using a very short TR and radio-frequency pulses with large flip angles. Although the 3D-bTFE sequence is susceptible to artifacts, it provides a relatively short scanning time compared with the fast spin-echo sequence.[18] In this study, the 3D-bTFE sequence was sufficient to evaluate the cranial nerves at the cisternal segment in most patients, but occasionally had to be replaced by the fast spin-echo sequence (ie, T2 VISTA) in patients with severe artifacts related to hyperpneumatization of the sphenoid sinus. The use of these techniques allowed the acquisition of MR images that were sufficient to examine abnormalities associated with ocular motor nerves.

Various abnormalities of the ocular motor nerves, orbit, and brain were found in congenital or developmental neuropathic strabismus in this investigation. The most common pathology is a motor nerve abnormality with innervations disorder, referred to as a congenital cranial dysinnervation disorder. Cranial dysinnervation disorders are primarily caused by neurogenic disturbances in the brain stem or in cranial nerve development, and, recently, several genetic abnormalities that affect brain stem and/or cranial nerve development have been found.[19]

Among the ocular motor nerve abnormalities, CNIV aplasia was the most common abnormality. This finding is concordant with previous reports in which CNIV palsy forms the largest proportion of congenital neuropathic strabismus.[11,13]

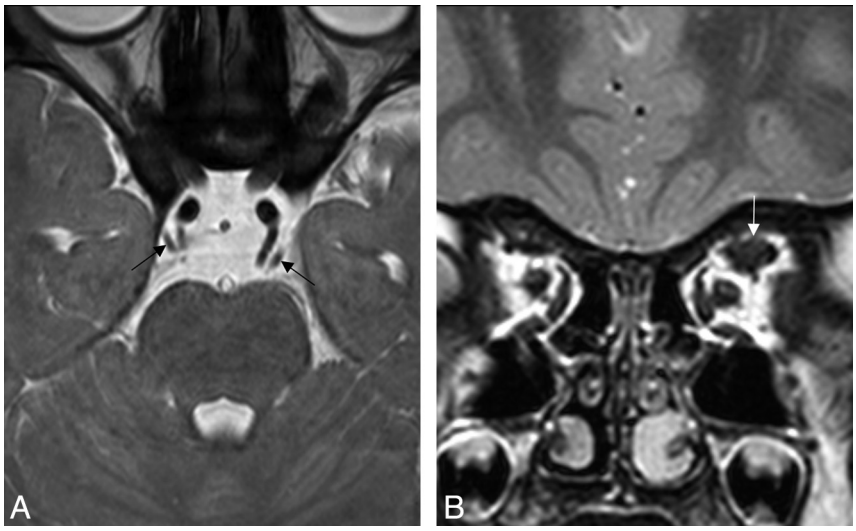

Fig 5. Superior rectus hypertrophy in a 3-year-old boy. *A,* Conventional-resolution 3D-bTFE image at the level of the upper pons shows a normal-size CNIII, bilaterally (*arrows*). *B,* Coronal T2-weighted image of the orbit shows a hypertrophic left superior rectus (*arrow*).

In the study by Demer et al,[11] the hypoplasia or absence of the superior oblique was found in approximately half of the patients with neuropathic strabismus; however, the authors did not consistently evaluate the status of CNIV. The present study, using high-resolution MR imaging, showed that superior oblique hypoplasia in all patients was associated with CNIV aplasia, except in 4 patients who had motion artifacts or a narrow cisternal space. However, the possibility of severe hypoplasia of CNIV (ie, CNIV is not detected because the nerve is smaller than the section thickness of the MR images) cannot be excluded because of the current MR image resolution.

The second most commonly observed location for abnormalities of the ocular motor nerves was CNVI. Most of these abnormalities involved CNVI aplasia, and all were clinically consistent with type 1 Duane retraction syndrome.[5,6,11] Interestingly, however, hypoplasia of the related lateral rectus was not associated with CNVI aplasia or hypoplasia. This may be attributed to aberrant innervation of the lateral rectus by a branch of CNIII.[20,21]

CNIII was the least affected nerve among the ocular motor nerves. CNIII normally divides into superior and inferior branches within the superior orbital fissure, and then enters the annulus of Zinn at the orbital apex. The superior branch innervates the superior rectus and the levator palpebrae superioris, while the inferior branch innervates the inferior rectus, the medial rectus, and the inferior oblique.[22] In the current study, 1 patient with CNIII aplasia had hypoplasia of all related EOMs. Two patients with CNIII hypoplasia had hypoplasia of the medial rectus and/or the inferior rectus, suggesting a localized defect of the CNIII inferior branch innervating the associated EOMs.[1,11] Another patient with bilateral CNIII hypoplasia, combined with CNVI aplasia, had hypoplasia of the superior rectus and the medial rectus bilaterally, possibly reflecting a similar type of localized defects at the CNIII branches.

Orbital abnormalities consisted of EOM hypoplasia and hypertrophy, as well as the presence of an orbital fibrotic mass. Four patients had unilateral superior oblique hypoplasia, but the presence or absence of CNIV could not be determined in these patients. Therefore, the possibility of EOM hypoplasia secondary to CNIV aplasia, as in the previously described patients, cannot be excluded. The 3 other patients with hypoplasia of other EOMs had normal-size ocular motor nerves at their cisternal segments. In a previous study involving the use of high-resolution orbital MR imaging, hypoplasia of the CNIII inferior branches in the orbit was found in 1 patient with corresponding EOM hypoplasia.[11] Therefore, EOM hypoplasia in the current study might also be caused by a deficiency of neural innervation rather than a primary myopathy. We speculate that CNIII associated with a single EOM hypoplasia can be normal in size at its cisternal segment because the neural fibers innervating other EOMs are preserved. On the other hand, the superior rectus hypertrophy and the orbital fibrotic mass found in this study seem to be rare abnormalities that have never been reported as causes of congenital or developmental strabismus.

Strabismus was found to be associated with periventricular leukomalacia in 4 patients and with periventricular heterotopia in 1 patient in our study population. Periventricular leukomalacia is an important cause of pediatric strabismus.[23-25] It was assumed that ischemic lesions in the occipital periventricular region, where afferent, efferent, and commissural fiber pathways of the visual cortex are located, may affect the visuomotor control system.[25] However, no study has examined the pathogenesis of strabismus in periventricular heterotopia. We speculate that heterotopia involving the occipital periventricular region may also affect the visuomotor control system, as in periventricular leukomalacia. However, it is uncertain whether periventricular leukomalacia involving other locations apart from the occipital region could be associated with development of strabismus. There should be further study of the relation between the location involved in periventricular leukomalacia and development of strabismus.

Structural abnormalities were not disclosed in approximately half of our patients with congenital or developmental neuropathic strabismus. Yang et al[3] also reported congenital superior oblique palsy without either CNIV aplasia or supe-

rior oblique hypoplasia. These authors suggested abnormal superior oblique tendon or pulley dysfunction as the putative cause of palsy. Huber[26] previously proposed that an anomalous branch of CNIII to the lateral rectus could be important in the etiology of type 2 Duane retraction syndrome. In this syndrome, MR imaging has recently shown the presence of CNVI and a normal-size lateral rectus.[10] Therefore, it is assumed that abnormalities of the nervous system or EOM, which are difficult to distinguish by the current MR imaging techniques, may cause strabismus in these patients. Further studies, including orbital nerve branch imaging or functional imaging of EOM contractility, might be helpful for investigating these unproven etiologies.

Our study has some limitations. First, midway in our study, we changed the 8-channel head coil to the 32-channel head coil, with subsequent modification of the MR protocol, for evaluating CNIV. Because of a better signal-to-noise ratio with the 32-channel coil, some parameters related to scan time were adjusted, keeping the voxel size constant. Therefore, it does not seem that the changed MR protocols influenced the results significantly. Second, the number of patients in the control group was small. With this small sample size, however, we think it is possible to show evidence that CNIII and CNVI were generally larger than CNVIII and CNIV, respectively, in diameter. Next, hypoplasia was defined when CNIII was smaller than CNVIII, and CNVI smaller than CNIV, respectively. However, we might have missed a mild degree of nerve hypoplasia with our method.

Conclusions

Various MR imaging abnormalities were identified in approximately half of the patients with congenital or developmental neuropathic strabismus. Ocular motor nerve abnormalities were the most common, followed by EOM abnormalities and brain abnormalities. CNIV aplasia was the most frequent abnormality, comprising 63% of all MR imaging abnormalities.

References

1. Kau HC, Tsai CC, Ortube MC, et al. **High-resolution magnetic resonance imaging of the extraocular muscles and nerves demonstrates various etiologies of third nerve palsy**. *Am J Ophthalmol* 2007;143:280–87
2. Kim JH, Hwang JM. **Absence of the trochlear nerve in patients with superior oblique hypoplasia**. *Ophthalmology* 2010;117:2208–13
3. Yang HK, Kim JH, Hwang JM. **Congenital superior oblique palsy and trochlear nerve absence: a clinical and radiological study**. *Ophthalmology* 2012;119:170–77
4. Kim JH, Hwang JM. **Hypoplastic oculomotor nerve and absent abducens nerve in congenital fibrosis syndrome and synergistic divergence with magnetic resonance imaging**. *Ophthalmology* 2005;112:728–32
5. Kim JH, Hwang JM. **Usefulness of MR imaging in children without characteristic clinical findings of Duane's retraction syndrome**. *AJNR Am J Neuroradiol* 2005;26:702–05
6. Kim JH, Hwang JM. **Presence of the abducens nerve according to the type of Duane's retraction syndrome**. *Ophthalmology* 2005;112:109–13
7. Ela-Dalman N, Velez FG, Demer JL, et al. **High-resolution magnetic resonance imaging demonstrates reduced inferior oblique muscle size in isolated inferior oblique palsy**. *J AAPOS* 2008;12:602–07
8. Clark RA, Miller JM, Rosenbaum AL, et al. **Heterotopic muscle pulleys or oblique muscle dysfunction?** *J AAPOS* 1998;2:17–25
9. Lim KH, Engle EC, Demer JL. **Abnormalities of the oculomotor nerve in congenital fibrosis of the extraocular muscles and congenital oculomotor palsy**. *Invest Ophthalmol Vis Sci* 2007;48:1601–06
10. Kim JH, Hwang JM. **Abducens nerve is present in patients with Type 2 Duane's retraction syndrome**. *Ophthalmology* 2012;119:403–06
11. Demer JL, Ortube MC, Engle EC, et al. **High-resolution magnetic resonance imaging demonstrates abnormalities of motor nerves and extraocular muscles in patients with neuropathic strabismus**. *J AAPOS* 2006;10:135–42
12. Jiao YH, Zhao KX, Wang ZC, et al. **Magnetic resonance imaging of the extraocular muscles and corresponding cranial nerves in patients with special forms of strabismus**. *Chin Med J (Engl)* 2009;122:2998–3002
13. Holmes JM, Mutyala S, Maus TL, et al. **Pediatric third, fourth, and sixth nerve palsies: a population-based study**. *Am J Ophthalmol* 1999;127:388–92
14. Ettl A, Salomonowitz E. **Visualization of the oculomotor cranial nerves by magnetic resonance imaging**. *Strabismus* 2004;12:85–96
15. Choi BS, Kim JH, Jung C, et al. **High-resolution 3D MR imaging of the trochlear nerve**. *AJNR Am J Neuroradiol* 2010;31:1076–79
16. Tsuchiya K, Aoki C, Hachiya J. **Evaluation of MR cisternography of the cerebellopontine angle using a balanced fast-field-echo sequence: preliminary findings**. *Eur Radiol* 2004;14:239–42
17. Ciftci E, Anik Y, Arslan A, et al. **Driven equilibrium (drive) MR imaging of the cranial nerves V-VIII: comparison with the T2-weighted 3D TSE sequence**. *Eur J Radiol* 2004;51:234–40
18. Jung NY, Moon WJ, Lee MH, et al. **Magnetic resonance cisternography: comparison between 3-dimensional driven equilibrium with sensitivity encoding and 3-dimensional balanced fast-field echo sequences with sensitivity encoding**. *J Comput Assist Tomogr* 2007;31:588–91
19. Oystreck DT, Engle EC, Bosley TM. **Recent progress in understanding congenital cranial dysinnervation disorders**. *J Neuroophthalmol* 2011;31:69–77
20. Hotchkiss MG, Miller NR, Clark AW, et al. **Bilateral Duane's retraction syndrome. A clinical-pathologic case report**. *Arch Ophthalmol* 1980;98:870–74
21. Miller NR, Kiel SM, Green WR, et al. **Unilateral Duane's retraction syndrome (Type 1)**. *Arch Ophthalmol* 1982;100:1468–72
22. Casselman J, Mermuys K, Delanote J, et al. **MRI of the cranial nerves–more than meets the eye: technical considerations and advanced anatomy**. *Neuroimaging Clin N Am* 2008;18:197–231
23. Jacobson L, Ygge J, Flodmark O, et al. **Visual and perceptual characteristics, ocular motility and strabismus in children with periventricular leukomalacia**. *Strabismus* 2002;10:179–83
24. Jacobson LK, Dutton GN. **Periventricular leukomalacia: an important cause of visual and ocular motility dysfunction in children**. *Surv Ophthalmol* 2000;45:1–13
25. Ohtsuki H, Yoshifumi K, Hasebe S, et al. **Comparative study of brain lesions detected by magnetic resonance imaging between strabismus and nonstrabismus in infancy**. *Ophthalmologica* 2000;214:105–10
26. Huber A. **Electrophysiology of the retraction syndromes**. *Br J Ophthalmol* 1974;58:293–300